

Go-Smart: Web-based Computational Modeling of Minimally Invasive Cancer Treatments

Phil Weir^{*}, Dominic Reuter[§], Roland Ellerweg[§], Tuomas Alhonnoro[†], Mika Pollari[‡], Philip Voglreiter[†], Panchatcharam Mariappan^{*}, Ronan Flanagan^{*}, Chang Sub Park[¶], Stephen Payne[¶], Elmar Staerk[§], Peter Voigt^{||}, Michael Moche^{||}, and Marina Kolesnik[§]

^{*} NUMA Engineering Services Ltd., Dundalk, Ireland

[†] Technical University of Graz, Graz, Austria

[‡] Aalto University, Helsinki, Finland

[§] Fraunhofer Institute for Applied Information Technology, Germany

[¶] University of Oxford, Oxford, United Kingdom

^{||} Leipzig University, Germany

Abstract—The web-based Go-Smart environment is a scalable system that allows the prediction of minimally invasive cancer treatment. Interventional radiologists create a patient-specific 3D model by semi-automatic segmentation and registration of pre-interventional CT (Computed Tomography) and/or MRI (Magnetic Resonance Imaging) images in a 2D/3D browser environment. This model is used to compare patient-specific treatment plans and device performance via built-in simulation tools. Go-Smart includes evaluation techniques for comparing simulated treatment with real ablation lesions segmented from follow-up scans. The framework is highly extensible, allowing manufacturers and researchers to incorporate new ablation devices, mathematical models and physical parameters.

Keywords: cancer, internet, image processing, simulation

I. INTRODUCTION

Minimally invasive cancer treatments (MICTs) represent a growing body of techniques for ablating cancerous tumors, avoiding major surgery. These MICT modalities include, among others, radiofrequency ablation (RFA), where percutaneous probes destroy tissue through Joule heating; microwave ablation (MWA), where dielectric heating is used; cryoablation, where tissue is lethally cooled; and irreversible electroporation (IRE), where the cell membrane is destroyed by an electric field. In a rapidly growing discipline, interventional radiologists (IRs) must remain informed about available treatments, as their MICT experience heavily influences patient outcomes [1]. Moreover, the boundaries of tissue necrosis are difficult to predict heuristically, and so experience is well complemented by medical simulation. In addition to single-modality offline workflows [2], [3], a multi-modality tool is thus required to flexibly compare a range of outcomes.

The Go-Smart¹ project (<http://gosmart-project.eu>) seeks to fulfill this, expanding on the RFA-specific IMPACT² project (<http://impact.eu>) [3], [4]. A web-based platform (<http://smart-mict.eu>) allows IRs to upload patient images,

¹Project Go-Smart is co-funded by the 7th Framework Programme of the European Union under Grant Agreement No: 600641.

²Project IMPACT was co-funded by the 7th Framework Programme of the European Union under Grant Agreement No: 223877.



Figure 1. The 2D web-browser interface, showing image segmentation

and to plan, compare and validate treatment options (Fig. 1). Establishing a complete environment has required significant development, encompassing image segmentation, registration, simulation, modeling and visualization, brought together within a purpose-built scalable web architecture. Underpinning Go-Smart is the principle that key MICTs share clinical and modeling commonalities. By exploiting this, a generic computational framework (Fig. 2) has been defined and adapted to multiple MICT modalities. A core feature of this framework is its extensibility; mathematical models, numerical codes, equipment and even modalities may be added through the interface, by independent researchers and manufacturers.

Pseudonymized validation data, for quantifying the performance of the image manipulation and simulation components, is provided by clinical partners, alongside a *Case Report Form* (CRF) containing all patient-specific data needed for simulation. It is intended that the environment will support independent evaluation of equipment, training of IRs, collaboration on treatment planning and medical research.

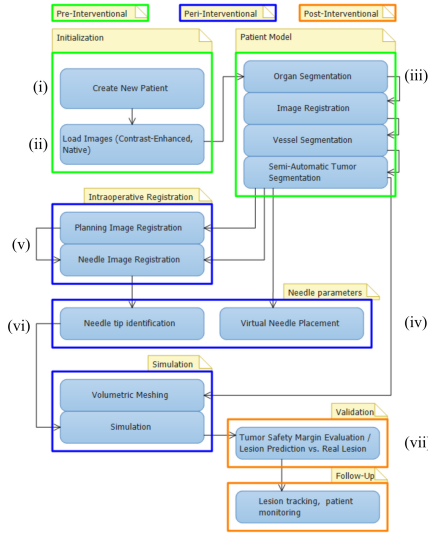


Figure 2. Go-Smart framework: i) Create project; ii) View data; iii) Segment; iv) Place virtual needles; v) Simulate; vi) Register needles; vii) Validate

II. USAGE

A. Clinicians

Initially, IRs add a new patient with basic personal details (Fig. 2.i). Pre-interventional CT and/or MRI images may be attached to the patient data and viewed in both 2D and 3D (Fig. 2.ii). Visible structures, such as the target organ, tumors and vessels are segmented semi-automatically using a collection of image analysis tools (Fig. 1; Fig. 2.iii), resulting in a patient-specific 3D model of critical structures. Regions where trans-arterial chemoembolization (TACE) has been applied, blocking blood supply to a tumor, may also be segmented.

Before performing an intervention, IRs place virtual probes in the segmented image, indicating the planned target (Fig. 2.iv). Equipment parameters and treatment protocols are input, then a simulation is executed, which estimates the lesion to be created (Fig. 2.v). This step normally takes 10-20 minutes, with variation for certain protocols, equipment and modalities. After the procedure, IRs upload intra-operative scans, which are registered to the pre-operative images, generating ablation probe coordinates within the original patient model. The IR may re-run the simulation with these real, measured probe locations (Fig. 2.vi). The physical lesion is segmented from follow-up scans performed 1-month post-intervention, and quantitatively compared to the prediction (Fig. 2.vii).

B. Researchers, developers and manufacturers

For each treatment modality, manufacturers provide guidance for IRs, often as complex algorithms, involving heating or cooling steps governed by time, electrical impedance and/or reported temperature. The environment incorporates these treatment protocols, simulating an IR or generator's behavior.

Researchers, developers and manufacturers may use the site's *Developer Corner* to add such treatment protocols, numerical models (e.g. an Elmer input file), or equipment. All

models, probes, power generators, organs and protocols have parameters, modifiable through this interface, which may also be set to prompt for case-specific clinician input.

III. IMPLEMENTATION

A. Distributed Architecture

The Go-Smart distributed design is optimized for stability and scalability. Allowing for computationally intensive workflow steps, processing is spread between machines. The architecture is divided into independent, separately-reusable components with clearly defined interfaces, as follows:

- **Clients:** browser; *Visapp* (Go-Smart 3D Support);
- **Servers:** web server; image processing server; segmentation/registration server; simulation server.

Microsoft ASP.NET SignalR (<http://signalr.net/>) provides reliable, rapid communication between services, allowing clients to interact directly with each component. Together they build up a resilient architecture, capable of handling substantial parallel workloads while retaining satisfactory user experience.

The web application delivers the user interface, as well as managing communication between all components. It supports multiple users and scalability via a separately-hostable microservice. The database and CDM (Sec. III-F) are also hosted here, as are patient images, 3D models and simulation results.

B. Browser Client

A standard web browser is sufficient to access Go-Smart, providing users with roaming access to patient data. The integrated viewer allows visual inspection of all data generated during the workflow in a 2D, slice-based representation, with axial, sagittal and coronal image windows. These can embed segmented and simulated surfaces into an image (Fig. 1). Key tools, such as image contrast windowing, provide a familiar radiology workspace, comparable to established applications.

C. Visapp Visualization Technology

The optional client application provides seamlessly integrated 3D visualization techniques, exploiting the local computing power of the client PC to minimize response times. The client's embedded web browser replaces the deactivated fourth view with a 3D render widget. Interaction with the underlying web page is immediately reflected in the embedded 3D viewer when required. The advanced 3D volume rendering techniques employed adjust to the specifications of the local hardware. From basic direct volume ray casting [5] to high-end global illumination techniques [6], a variety of options are supplied to the user. We incorporate both volumetric data and surface-based representation of segmentation, simulation results and MICT probes, for exploring treatment possibilities and evaluation purposes, supplementing the standard 2D views.

D. Image Processing Server

This component supports the client viewer, providing image re-slicing. All image editing tools are integrated here, such as contrast setting, segmentation editing and needle placement.

E. Image Segmentation and Registration

Within this component, the patient-specific 3D model is built using purpose-built tools. First, separate images are registered into a common coordinate system using multimodal semi-automatic registration. As well as breath-hold compensation between consecutive contrast-enhanced sequences, registration of intra-operative (needle) images and post-operative follow-up validation images to pre-operative images is also implemented. The target organ is automatically segmented through organ-specific tools, using a rough decomposition of abdominal structures into semantic objects and morphology-based segmentation. For certain organs and lesions, single-click initialization is used for robustness, supplemented by ‘drawing’ tools for manual correction. Internal tubular structures, such as vessels, bile ducts and bronchi, are extracted by an altering Hessian vessel model based segmentation method.

F. Clinical Domain Model (CDM)

The Clinical Domain Model, a conceptual framework, gives separate identities to components: numerical models, equipment, organs and protocols, each of which maintains a set of parameters. Their relationships and allowed combinations are modified through a *Developer Corner* web-interface. Composition rules enable interchangeability of individual components.

G. Simulation Architecture (GSSA)

The simulation architecture is a self-contained framework marshaled by a CDM-produced XML file. It contains a fully-automated, configurable tool-chain, with volumetric meshing by CGAL [7] and simulation by Elmer (<https://www.csc.fi/web/elmer>). New sandboxed numerical codes may be added to GSSA using a Docker container (<http://www.docker.com>) and gluing Python module. An OpenFOAM container (<http://www.openfoam.com>) and a Python/FEniCS [8] container have been implemented, allowing interface users to run their own Python-based models.

IV. MATHEMATICAL MODELS

Models used for simulating key modalities are outlined. For rigorous discussion of the theory, we refer to [9].

A. Common Models of Thermal Modalities

1) *Bioheat equation with perfusion term*: Following IMPACT [3], [4], and Kröger et al. [10], a Pennes bioheat equation with perfusion term is used for thermal modalities [9], [11]. The governing volumetric equation in the tissue is,

$$\rho c \partial_t T - k \nabla^2 T = Q_{\text{inst}} + Q_{\text{perf}}, \quad (1)$$

where ρ , c , k and T are the density (kg m^{-3}), specific heat capacity ($\text{J kg}^{-1} \text{K}^{-1}$), thermal conductivity ($\text{W m}^{-1} \text{K}^{-1}$) and temperature of tissue (K), respectively. Q_{inst} is the heat absorbed due to ablation (W m^{-3}). Q_{perf} is proportional to deviation from 310 K, with a tissue-type dependent factor.

2) *Cell death model*: For hyperthermia, a three-state cell death model is used [11], [12]. Locally, cells are divided between three states: Alive (A), Vulnerable (V) or Dead (D). At each point, changes of state over time follow the rules,

$$A \leftrightarrow V \rightarrow D, \quad A + V + D = 1, \quad (2)$$

according to coupled evolution equations with T -dependent coefficients. The lesion is defined as $\Sigma := \{D \geq 0.8\}$.

B. MICT-Specific Models

1) *Microwave ablation*: This modality is modeled by coupling the above bioheat and death equations to a reduced form of Maxwell’s equations, using a transverse-magnetic (TM) axisymmetric cylindrical solver with temperature-dependent electromagnetic parameters [9], [13], [14]. The field may be used to estimate the specific absorption rate of the tissue.

2) *Cryoablation*: A front-capturing multi-phase solver is applied to the Pennes equation to ensure the accuracy of physical properties changing due to the expanding ice ball. The *effective heat capacity method* is used, incorporating latent heat of phase change into c and adjusting k . This admits a *mushy* transition region between solid and liquid states [9], [15]. The effective values are inserted into the bioheat equation and the resulting nonlinear problem is solved iteratively.

3) *Irreversible electroporation*: For each step, i , in the protocol, IRE is modeled using a simple electric potential solver, with potential along the i^{th} anode equal to the i^{th} potential difference, and zero potential along the i^{th} cathode. The final lesion is defined as an isovolume of the local energy maximum over the whole protocol sequence [9], [16].

4) *Radiofrequency ablation*: Rather than simulating Joule heating for each execution of this modality, an empirical approach is used, consisting of a summation of Gaussian functions centered on suitably chosen points. This was validated during the IMPACT project, and avoids the oversized meshes required to capture < 1 mm diameter probe tines [4].

V. VALIDATION

The clinical partners of the project supply validation data for the modalities described in detail above, all uploaded and segmented by an experienced IR through the standard interface. Validation measures include the well-established average absolute error, α and target overlap, ϕ_S [17]. For a simulated lesion, Σ , and segmented lesion, S , the absolute error at a point on ∂S is the minimum distance to a point on $\partial \Sigma$. α is then the surface integral of these values divided by the area of ∂S . ϕ_S is defined as the volumetric ratio, $|S \cap \Sigma|/|S|$.

The tool minimizes α over rigid motions of S , offsetting post-operative registration errors. While this approach isolates inaccuracies due to the normal clinical workflow, ϕ_S , being independent, becomes a more useful comparative measure. To demonstrate the process, sample cases are presented in Tab. I.

While underestimation is shown by $\phi_S \ll 1.0$, overestimation, where $S \ll \Sigma$, is indicated by large α and $\phi_S \lesssim 1.0$. From Tab. I, it is seen that the RFA samples are particularly well-matched, with $\phi_S > 0.7$ and $\alpha < 2.5$ in both cases

Table I
VALIDATION MEASURES FOR 8 CASES (3 S.F.)

Modality	Cryo.	IRE	RFA	MWA
Organ	Kidney	Liver	Liver	Liver
1. α (mm)	3.04	5.33	2.46	1.26
ϕ_S	0.953	0.357	0.701	0.593
2. α (mm)	1.95	3.28	2.01	1.41
ϕ_S	0.675	0.866	0.711	0.803

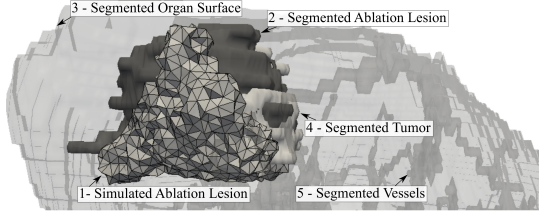


Figure 3. Validation case RFA.1 showing simulated (1) and segmented (2) lesions, in a segmented liver (3) with tumor (4) and vessel structure (5)

(Fig. 3). RFA benefits from longstanding project experience and well-tested empirical parameters. IRE.1, in contrast, shows $\alpha \gg 1$ and, for IRE.2, $\phi_S \ll 1$. Often measured IRE lesions are small, and may require fuller modeling of device settings. Although MWA.2 is adequate, MWA.1 underestimates, with $\phi_S < 0.6$. This may be related to probe idiosyncrasies, fundamental to MWA, and rectified through further tailored equipment modeling. Cryo.1 is overestimated, with $\alpha \gg 1$ and $\phi_S \approx 1$, while Cryo.2 is underestimated, with $\phi_S \ll 1$. Many treated kidney tumors are exophytic, with ablations close to the organ wall, a limit of the simulation domain, Ω . $|\Sigma|$ is thus sensitive to needle placement error, arising from intra-operative to pre-operative image registration. To resolve this, Ω may be extended beyond the organ. Using Go-Smart's model extensibility, such changes may be made through the web interface or back-end. As the overall validation error has two main computational sources, image processing and simulation, we cannot reliably distinguish their contributions. Yet some analysis is possible. Between liver cases, the error shown is higher for MWA and IRE than for RFA, while image processing steps are the same, implying simulation inaccuracy.

VI. CONCLUSION

The Go-Smart web environment has been presented. It allows IRs to simulate treatment for multiple MICT modalities and target organs, through a web-based interface. The core simulation codes are then validated against IR-segmented ablation lesions. As an open-ended system, researchers and manufacturers are able to extend the framework with additional equipment, treatment protocols and numerical models.

This framework represents a culmination of novel work covering web infrastructure, image segmentation, image registration, theoretical modeling, visualization techniques and simulation, both extending and integrating underlying open source solvers. Potential applications in e-health include international collaboration on treatment planning, establishing a baseline for

MICT training and independent assessment of new equipment and techniques against an existing body of data.

ACKNOWLEDGMENTS

This research was funded by the European Commission, under Grant Agreement no. 600641, FP7 Project Go-Smart. The authors gratefully acknowledge the significant contribution to this project made by our clinical partners at Leipzig University, Medical University of Graz, Radboud University Medical Centre Nijmegen and University Hospital Frankfurt.

REFERENCES

- [1] P. Hildebrand, T. Leibecke, M. Kleemann, L. Mirow, M. Birth, H. Bruch, and C. Bürk, "Influence of operator experience in radiofrequency ablation of malignant liver tumours on treatment outcome," *Eur. J. Surg. Oncol. (EJSO)*, vol. 32, no. 4, pp. 430–434, 2006.
- [2] C. Rieder, T. Kröger, C. Schumann, and H. K. Hahn, "GPU-based real-time approximation of the ablation zone for radiofrequency ablation," *IEEE Trans. Comput. Graph.*
- [3] B. Kerbl, P. Voglreiter, R. Khlebnikov, D. Schmalstieg, D. Seider, M. Moche, P. Stiegler, R. H. Portugaller, and B. Kainz, "Intervention planning of hepatocellular carcinoma radio-frequency ablations," in *Clinical Image-Based Procedures. From Planning to Intervention*, pp. 9–16, Springer, 2013.
- [4] S. Payne, R. Flanagan, M. Pollari, T. Alhonnoro, C. Bost, D. O'Neill, T. Peng, and P. Stiegler, "Image-based multi-scale modelling and validation of radio-frequency ablation in liver tumours," *Phil. Trans. R. Soc. Lond. A*, vol. 369, no. 1954, pp. 4233–4254, 2011.
- [5] M. Levoy, "Efficient ray tracing of volume data," *ACM Transactions on Graph. (TOG)*, vol. 9, no. 3, pp. 245–261, 1990.
- [6] R. Khlebnikov, P. Voglreiter, M. Steinberger, B. Kainz, and D. Schmalstieg, "Parallel irradiance caching for interactive Monte-Carlo direct volume rendering," in *Computer Graphics Forum*, vol. 33, pp. 61–70, Wiley Online Library, 2014.
- [7] The CGAL Project, *CGAL User and Reference Manual*. CGAL Editorial Board, 2015.
- [8] A. Logg, K.-A. Mardal, G. N. Wells, et al., *Automated Solution of Differential Equations by the Finite Element Method*. Springer, 2012.
- [9] S. K. Hall, E. H. Ooi, and S. J. Payne, "A mathematical framework for minimally invasive tumor ablation therapies," *Critical Rev. Biomed. Eng.*, vol. 42, no. 5, 2014.
- [10] T. Kröger, I. Altrogge, T. Preusser, P. L. Pereira, D. Schmidt, A. Weihusen, and H.-O. Peitgen, "Numerical simulation of radio frequency ablation with state dependent material parameters in three space dimensions," in *Medical Image Computing and Computer-Assisted Intervention-MICCAI 2006*, pp. 380–388, Springer, 2006.
- [11] S. K. Hall, E. H. Ooi, and S. J. Payne, "Cell death, perfusion and electrical parameters are critical in models of hepatic radiofrequency ablation," *Int. J. Hyperth.*, no. in press, pp. 1–13, 2015.
- [12] D. P. O'Neill, T. Peng, P. Stiegler, U. Mayrhauser, S. Koestenbauer, K. Tscheliessnigg, and S. J. Payne, "A three-state mathematical model of hyperthermic cell death," *Ann. Biomed. Eng.*, vol. 39, no. 1, pp. 570–579, 2011.
- [13] J. M. Bertram, D. Yang, M. C. Converse, J. G. Webster, and D. M. Mahvi, "Antenna design for microwave hepatic ablation using an axisymmetric electromagnetic model," *Biomed. Eng. Online*, vol. 5, no. 15, pp. 24–29, 2006.
- [14] Z. Ji and C. L. Brace, "Expanded modeling of temperature-dependent dielectric properties for microwave thermal ablation," *Phys. medicine biology*, vol. 56, no. 16, p. 5249, 2011.
- [15] Z.-S. Deng and J. Liu, "Modeling of multidimensional freezing problem during cryosurgery by the dual reciprocity boundary element method," *Eng. Analysis with Boundary Elem.*, vol. 28, no. 2, pp. 97–108, 2004.
- [16] P. A. Garcia, R. V. Davalos, and D. Miklavcic, "A numerical investigation of the electric and thermal cell kill distributions in electroporation-based therapies in tissue," *PLoS ONE*, vol. 9, no. 8, 2014.
- [17] A. Klein, J. Andersson, B. A. Ardekani, J. Ashburner, B. Avants, M.-C. Chiang, G. E. Christensen, D. L. Collins, J. Gee, P. Hellier, et al., "Evaluation of 14 nonlinear deformation algorithms applied to human brain MRI registration," *Neuroimage*, vol. 46, no. 3, pp. 786–802, 2009.